Electronic properties of graphene and graphene nanoribbons with 'pseudo-Rashba' spin-orbit coupling

2009 New J. Phys. 11 115003

(http://iopscience.iop.org/1367-2630/11/11/115003)

New Journal of Physics
The open-access journal for physics

Electronic properties of graphene and graphene nanoribbons with 'pseudo-Rashba' spin-orbit coupling

Tobias Stauber[1] **and John Schliemann**[2]

[1] Departamento de Fsica Centro de Fsica, Universidade do Minho, P-4710-057 Braga, Portugal
[2] Institute for Theoretical Physics, University of Regensburg, D-93040 Regensburg, Germany
E-mail: tobias.stauber@fisica.uminho.pt

New Journal of Physics **11** (2009) 115003 (21pp)
Received 8 June 2009
Published 2 November 2009
Online at http://www.njp.org/
doi:10.1088/1367-2630/11/11/115003

Abstract. We discuss the electronic properties of graphene and graphene nanoribbons including 'pseudo-Rashba' spin–orbit coupling. After summarizing the bulk properties of massless and massive Dirac particles, we first analyze the scattering behavior close to an infinite mass and zigzag boundary. For low energies, we observe strong deviations from the usual spin-conserving behavior at high energies such as reflection acting as a spin polarizer or switch. This results in spin polarization along the direction of the boundary due to the appearance of evanescent modes in the case of non-equilibrium or when there is no coherence between the two one-particle branches. We then discuss the spin and density distribution of graphene nanoribbons.

Contents

1. Introduction **2**
2. Dirac fermions with 'pseudo-Rashba' spin–orbit coupling **3**
3. Spin dephasing due to reflection on a hard wall **5**
3.1. Infinite mass boundary 6
3.2. Zigzag boundary 11
4. Spin polarization close to the boundary **12**
5. Dirac electrons with 'pseudo-Rashba' spin–orbit coupling in nanoribbons **14**
5.1. Quantization of the transverse momentum 14
5.2. Spin and density distribution 16
6. Summary **17**
Acknowledgments **18**
Appendix A. The full model including the two *K*-points **18**
Appendix B. Massive Dirac fermions with 'pseudo-Rashba' spin–orbit coupling **18**
Appendix C. Scattering from infinite mass boundary **20**
References **21**

1. Introduction

Graphene, the single-layer allotrope of carbon, is undoubtedly one of the most active fields in today's experimental and theoretical condensed matter physics [1]–[3]. Among an entire plethora of phenomena and proposals, the issue of spin–orbit coupling has generated particular interest [4]–[9]. A detailed understanding of spin–orbit interaction in graphene is crucial for the interpretation of ongoing experiments on spin transport performed by various groups [10]–[18]. Other issues include various device proposals [19, 20] and theoretical predictions [21]–[23] related to spins and spin–orbit coupling in graphene.

In the present paper we investigate a single layer of graphene in the presence of spin–orbit interaction of the 'pseudo-Rashba' type, coupling the sublattice or pseudo-spin to the physical electron spin [4]–[9], [24]. Our interest is based on the fact that for graphene on Ni with intercalation of Au, a 100-fold enhancement of 'pseudo-Rashba' spin–orbit coupling has been reported [25]. Furthermore, impurities that induce an sp3 distortion will lead to 'pseudo-Rashba' spin–orbit coupling with a value comparable to that found in diamond and other zinc-blende semiconductors [26]. The latter result indicates that the 'pseudo-Rashba' spin–orbit coupling can be controlled via impurity coverage.

In this paper, we will concentrate on the scattering behavior of spin densities near boundaries created by either an infinite mass or a zigzag edge. Our presentation is organized as follows: In section 2 we introduce the basic Hamiltonian and discuss its general bulk solution in the absence of a mass term; the technically more complicated case of a nonzero mass is deferred to the appendices. In section 3 we investigate in detail the scattering properties and spin dephasing at hard boundaries for various types of incoming spinors and energy ranges. This discussion is extended in section 4 to averaged spin polarizations obtained from continuous distributions of incoming directions. In section 5, we analyze the spin and density distribution

of graphene nanoribbons. We close with a summary in section 6. Throughout this manuscript, we use parameters of [25].

2. Dirac fermions with 'pseudo-Rashba' spin–orbit coupling

The single-particle Hamiltonian of monolayer graphene with 'pseudo-Rashba' spin–orbit interaction can be formulated as [4]–[6], [24]

$$\mathcal{H} = v_F \vec{p} \cdot \vec{\tau} + \lambda \, (\vec{\tau} \times \vec{\sigma}) \cdot \vec{e}_z, \tag{1}$$

where, among standard notation, λ is the spin–orbit coupling parameter, and the Pauli matrices $\vec{\tau}$, $\vec{\sigma}$ describe the sublattice and the electron spin degree of freedom, respectively. For a given wave vector $\vec{k}$, this Hamiltonian reads explicitly as

$$\mathcal{H}(\vec{k}) = \begin{pmatrix} 0 & 0 & \hbar v_F (k_x - \mathrm{i} k_y) & 0 \\ 0 & 0 & 2\mathrm{i}\lambda & \hbar v_F (k_x - \mathrm{i} k_y) \\ \hbar v_F (k_x + \mathrm{i} k_y) & -2\mathrm{i}\lambda & 0 & 0 \\ 0 & \hbar v_F (k_x + \mathrm{i} k_y) & 0 & 0 \end{pmatrix}. \tag{2}$$

From experience with the 'classic' Dirac equation of relativistic quantum mechanics, it is occasionally of use not to study just a given Hamiltonian but also its square. Here we find

$$\mathcal{H}^2(\vec{k}) = \begin{pmatrix} (\hbar v_F k)^2 & -2\mathrm{i}\lambda\hbar v_F (k_x - \mathrm{i} k_y) & 0 & 0 \\ 2\mathrm{i}\lambda\hbar v_F (k_x + \mathrm{i} k_y) & (\hbar v_F k)^2 + 4\lambda^2 & 0 & 0 \\ 0 & 0 & (\hbar v_F k)^2 + 4\lambda^2 & -2\mathrm{i}\lambda\hbar v_F (k_x - \mathrm{i} k_y) \\ 0 & 0 & 2\mathrm{i}\lambda\hbar v_F (k_x + \mathrm{i} k_y) & (\hbar v_F k)^2 \end{pmatrix}. \tag{3}$$

This matrix is block diagonal with eigenvalues

$$(\varepsilon^2)_{1,2} = (\hbar v_F k)^2 + 2\lambda^2 \pm 2|\lambda| \sqrt{(\hbar v_F k)^2 + \lambda^2}, \tag{4}$$

where the positive sign corresponds to the eigenvectors

$$|\alpha_1\rangle = \begin{pmatrix} \sin(\vartheta/2) \\ \cos(\vartheta/2) e^{\mathrm{i}\eta} \\ 0 \\ 0 \end{pmatrix}, \quad |\beta_1\rangle = \begin{pmatrix} 0 \\ 0 \\ \cos(\vartheta/2) \\ \sin(\vartheta/2) e^{\mathrm{i}\eta} \end{pmatrix}, \tag{5}$$

while for the negative sign we have

$$|\alpha_2\rangle = \begin{pmatrix} \cos(\vartheta/2) \\ -\sin(\vartheta/2) e^{\mathrm{i}\eta} \\ 0 \\ 0 \end{pmatrix}, \quad |\beta_2\rangle = \begin{pmatrix} 0 \\ 0 \\ -\sin(\vartheta/2) \\ \cos(\vartheta/2) e^{\mathrm{i}\eta} \end{pmatrix}, \tag{6}$$

where $\vartheta \in [0, \pi]$ and

$$\cos\vartheta = \frac{|\lambda|}{\sqrt{(\hbar v_F k)^2 + \lambda^2}}, \quad e^{i\eta} = \frac{\lambda}{|\lambda|}\frac{i(k_x + ik_y)}{k}. \tag{7}$$

In the basis $(|\alpha_1\rangle, |\beta_1\rangle, |\alpha_2\rangle, |\beta_2\rangle)$ the Hamiltonian reads as

$$\tilde{\mathcal{H}}(\vec{k}) = \begin{pmatrix} 0 & q_+^* & 0 & 0 \\ q_+ & 0 & 0 & 0 \\ 0 & 0 & 0 & q_- \\ 0 & 0 & q_-^* & 0 \end{pmatrix} \tag{8}$$

with

$$q_\pm = \pm\hbar v_F (k_x \pm ik_y) f_\pm(|\lambda|/\hbar v_F k) \tag{9}$$

and

$$f_\pm(x) = \sqrt{1 + x^2} \pm x. \tag{10}$$

Now it is straightforward to obtain the full eigensystem: We find a gaped pair of eigenvalues

$$\varepsilon_{1,\pm} = \pm\left(\sqrt{(\hbar v_F k)^2 + \lambda^2} + |\lambda|\right) \tag{11}$$

with eigenspinors (type I)

$$|\chi_{1,\pm}(\vec{k})\rangle = \frac{1}{\sqrt{2}} \begin{pmatrix} \sin(\vartheta/2) \\ \cos(\vartheta/2)e^{i\eta} \\ \pm\cos(\vartheta/2)e^{i\psi} \\ \pm\sin(\vartheta/2)e^{i\eta}e^{i\psi} \end{pmatrix} \tag{12}$$

and

$$e^{i\psi} = \frac{k_x + ik_y}{k}. \tag{13}$$

With $g_V = 2$ being valley degeneracy, the corresponding density of states reads

$$\rho_1(\varepsilon) = \frac{g_V}{2\pi(\hbar v_F)^2}(|\varepsilon| - |\lambda|)\,\theta\left(\varepsilon^2 - (2\lambda)^2\right). \tag{14}$$

The other pair of dispersion branches does not exhibit a gap,

$$\varepsilon_{2,\pm} = \pm\left|\sqrt{(\hbar v_F k)^2 + \lambda^2} - |\lambda|\right|, \tag{15}$$

and has eigenspinors (type II)

$$|\chi_{2,\pm}(\vec{k})\rangle = \frac{1}{\sqrt{2}} \begin{pmatrix} \cos(\vartheta/2) \\ -\sin(\vartheta/2)e^{i\eta} \\ \pm\sin(\vartheta/2)e^{i\psi} \\ \mp\cos(\vartheta/2)e^{i\eta}e^{i\psi} \end{pmatrix}. \tag{16}$$

The corresponding density of states reads

$$\rho_2(\varepsilon) = \frac{g_V}{2\pi(\hbar v_F)^2}(|\varepsilon| + |\lambda|). \tag{17}$$

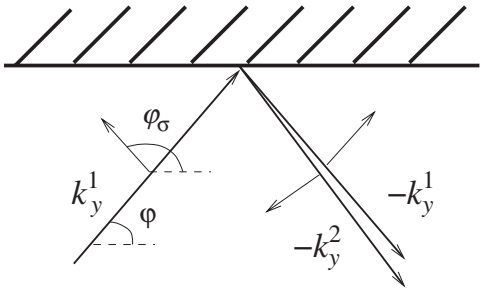

Figure 1. A plane wave of type I with spin perpendicular to the momentum $\vec{k} = (k_x, k_y^1)$ ($\varphi = \arctan(k_y^1/k_x)$, $\varphi_\sigma = \varphi + \pi/2$) is reflected at the boundary into a plane wave with $\vec{k}' = (k_x, -k_y^1)$ and $\vec{k}'' = (k_x, -k_y^2)$ with perpendicular spin, but anti-parallel with respect to each other (see equation (24) for the definition of $k_y^{1/2}$).

Let us now consider expectation values within the eigenstates with wave functions

$$\langle \vec{r}|\vec{k}, \mu, \pm\rangle = \frac{\mathrm{e}^{\mathrm{i}\vec{k}\vec{r}}}{\sqrt{\mathcal{A}}}|\chi_{\mu,\pm}\rangle, \tag{18}$$

$\mu \in \{1, 2\}$, and $\mathcal{A}$ being the area of the system. Here we find

$$\langle \vec{k}, 1, \pm|\vec{\tau}|\vec{k}, 1, \pm\rangle = \langle \vec{k}, 2, \pm|\vec{\tau}|\vec{k}, 2, \pm\rangle = \pm\frac{\lambda}{|\lambda|}\begin{pmatrix}\sin\vartheta\cos\varphi\\ \sin\vartheta\sin\varphi\\ 0\end{pmatrix} \tag{19}$$

and

$$\langle \vec{k}, 1, \pm|\vec{\sigma}|\vec{k}, 1, \pm\rangle = -\langle \vec{k}, 2, \pm|\vec{\sigma}|\vec{k}, 2, \pm\rangle = \frac{\lambda}{|\lambda|}\begin{pmatrix}-\sin\vartheta\sin\varphi\\ \sin\vartheta\cos\varphi\\ 0\end{pmatrix}. \tag{20}$$

Here, φ is the usual azimuthal angle of the wave vector, $\vec{k} = k(\cos\varphi, \sin\varphi)$. Note that

$$\langle\vec{\tau}\rangle \cdot \langle\vec{\sigma}\rangle = \vec{k} \cdot \langle\vec{\sigma}\rangle = 0, \tag{21}$$

as usual for Rashba spin–orbit coupling, and

$$|\langle\vec{\tau}\rangle| = |\langle\vec{\sigma}\rangle| = \sin\vartheta, \tag{22}$$

where for $\sin\vartheta < 1$ the sublattice and electron spin degree of freedom are entangled with each other.

3. Spin dephasing due to reflection on a hard wall

In this section, we will study the scattering behavior from a hard wall, which will lead to spin dephasing as depicted in figure 1. For that, a general plane wave with fixed momentum k_x and energy $E \geqslant 2|\lambda|$ is written as

$$\psi_{E,k_x}(x, y) = \mathcal{N}_{\vec{k}}\mathrm{e}^{\mathrm{i}k_x x}\Big[A_1\mathrm{e}^{\mathrm{i}k_y^1 y}|\chi_{1,+}(k_x, k_y^1)\rangle + A_2\mathrm{e}^{\mathrm{i}k_y^2 y}|\chi_{2,+}(k_x, k_y^2)\rangle$$
$$+R_1\mathrm{e}^{-\mathrm{i}k_y^1 y}|\chi_{1,+}(k_x, -k_y^1)\rangle + R_2\mathrm{e}^{-\mathrm{i}k_y^2 y}|\chi_{2,+}(k_x, -k_y^2)\rangle\Big], \tag{23}$$

with

$$(\hbar v_F k_y^{\mu})^2 = (E + (-1)^{\mu}|\lambda|)^2 - \lambda^2 - (\hbar v_F k_x)^2, \tag{24}$$

$\mu \in \{1, 2\}$ and the normalization constant $\mathcal{N}_{\vec{k}}$. For energies $E < 2|\lambda|$, some modifications in equation (23) have to be made, which shall be discussed in more detail below.

In the following, we will discuss reflection at a hard wall at $y = 0$ for the two types of plane waves i.e. we will first set $A_1 = 1$, $A_2 = 0$ (type I) and then $A_1 = 0$, $A_2 = 1$ (type II). The discussion is based on the reflected spin direction, which shall be denoted by φ'_σ. It is obtained from the expectation value of the spin-density operator at the boundary $\vec{\rho} = \vec{\sigma}\delta(\hat{\vec{r}})$, $\langle\vec{\rho}\rangle \equiv \langle\psi_{E,k_x}|\vec{\rho}|\psi_{E,k_x}\rangle$ via

$$\varphi'_\sigma = \arctan(\langle\rho_y\rangle/\langle\rho_x\rangle) + \pi\theta(-\langle\rho_x\rangle). \tag{25}$$

Owing to translational invariance in the x-direction, $\langle\vec{\rho}\rangle$ will only depend on the y-coordinate. For the following discussion, we will also discuss at $\vec{r} = 0$ the normalized expectation value $\langle\vec{\sigma}\rangle = \langle\vec{\rho}\rangle/\langle n\rangle$ with $\langle n\rangle \equiv \langle\psi_{E,k_x}|\delta(\hat{\vec{r}})|\psi_{E,k_x}\rangle$. This shall not be confused with the bulk expectation of $\vec{\sigma}$ as it appears in the Hamiltonian.

We will distinguish the two different cases of the half-plane $y \geqslant 0$ (scattering from the lower or bottom boundary) and $y \leqslant 0$ (scattering from the upper or top boundary). We shall further assume a plane wave with $k_x > 0$ moving in the positive x-direction. The results for $k_x < 0$ are then obtained by changing the bottom to top boundary and vice versa. The results for the K'-point can also be deduced from the following discussion (see appendix A). The sign of λ determines the sign of the expectation value of $\vec{\tau}$ and $\vec{\sigma}$. In the following, we set $\lambda = |\lambda|$, but in some of the following expressions we explicitly use $|\lambda|$ for the sake of clarity.

We will discuss two different types of confinement. First, we use the fact that Dirac fermions can be confined by an infinite mass boundary, first discussed by Berry and Mondragon [27]. We then also study the reflection from a zigzag boundary first addressed in [28].

3.1. Infinite mass boundary

With $\psi_{E,k_x} = (\psi_1, \psi_2, \psi_3, \psi_4)^{\mathrm{T}}$, the boundary conditions at the infinite mass boundary read (see appendices B and C) as

$$\left.\frac{\psi_1}{\psi_3}\right|_{\text{bottom}} = \left.\frac{\psi_2}{\psi_4}\right|_{\text{bottom}} = 1, \quad \left.\frac{\psi_1}{\psi_3}\right|_{\text{top}} = \left.\frac{\psi_2}{\psi_4}\right|_{\text{top}} = -1. \tag{26}$$

Note that there are different boundary conditions depending on whether one approaches the boundary from below or above.

3.1.1. Scattering behavior for plane waves of type I. We first consider a plane wave scattered at $y = 0$ with $A_1 = 1$ and $A_2 = 0$. The boundary conditions yield the following expressions for R_1, R_2:

$$R_1 = \mp z_1^2 \frac{(z_1c_1 \pm s_1)(z_2s_2 \pm c_2) + (z_1s_1 \pm c_1)(z_2c_2 \pm s_2)z_1z_2}{(z_1s_1 \pm c_1)(z_2s_2 \pm c_2)z_1 + (z_1c_1 \pm s_1)(z_2c_2 \pm s_2)z_2}, \tag{27}$$

$$R_2 = \mp z_2^2 \frac{(z_1c_1 \pm s_1)^2 - (z_1s_1 \pm c_1)^2 z_1^2}{(z_1s_1 \pm c_1)(z_2s_2 \pm c_2)z_1 + (z_1c_1 \pm s_1)(z_2c_2 \pm s_2)z_2}. \tag{28}$$

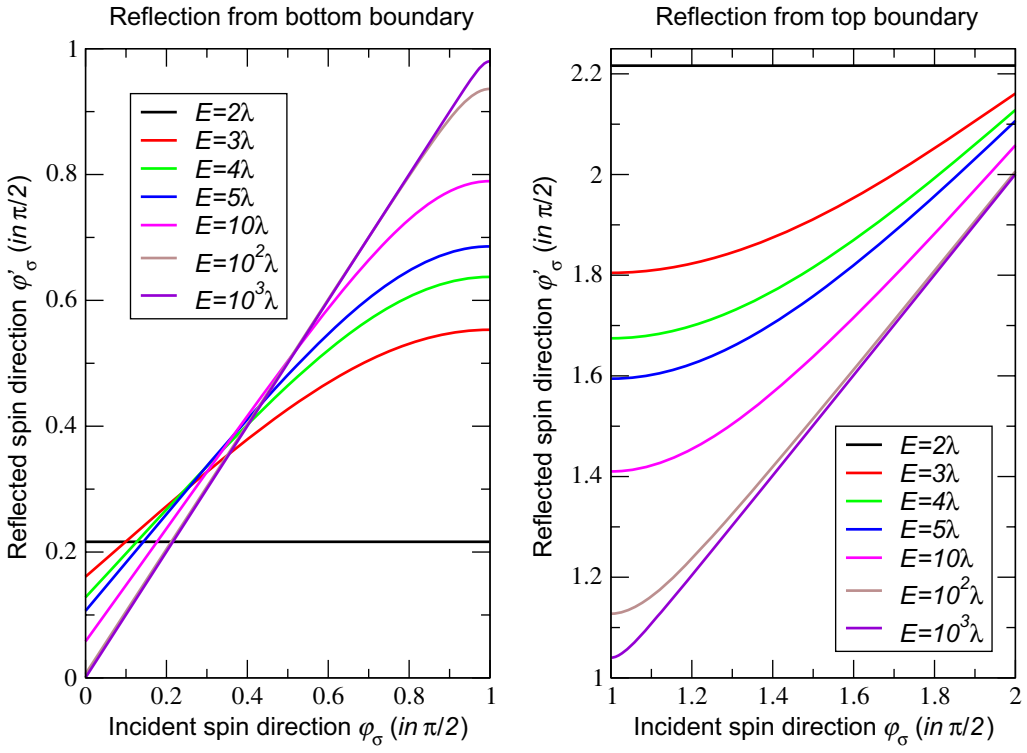

Figure 2. The reflected versus the incident spin direction at $y = 0$ for an incident plane wave with $A_2 = 0$ (type I) for various energies E. We use $\hbar v_F = 5.6\,\text{eV\AA}$ and $\lambda = 6\,\text{meV}$. Left: Reflection from the lower boundary. Right: Reflection from the upper boundary.

Above, we introduced the abbreviations $c_\mu = \cos(\vartheta_\mu/2)$, $s_\mu = \sin(\vartheta_\mu/2)$ and $z_\mu = (k_x + \mathrm{i}k_y^\mu)/\sqrt{k_x^2 + (k_y^\mu)^2}$, $\mu \in \{1, 2\}$. The upper (lower) sign holds if the electron is scattered from the upper (lower) boundary.

Let us first discuss the scattering behavior from the lower boundary. For $k_x = k\cos\varphi$, the incident spin direction is given by $\varphi_\sigma = \pi/2 - |\varphi|$. On the left-hand side of figure 2, the reflected spin direction φ'_σ of equation (25) is plotted against the incident spin direction φ_σ.

At large energies with $\epsilon = \lambda/(\hbar v_F k) \ll 1$ and $\epsilon \ll \sin^2\varphi$, we have $R_1 = (1-\epsilon)\cos\varphi$ and $R_2 = \mathrm{i}\sin\varphi - 2\epsilon\cos\varphi$ and the spin polarization is approximately conserved. The expansion of equation (25) yields

$$\varphi'_\sigma = \varphi_\sigma + \epsilon\frac{\cos\varphi_\sigma}{1+\sin\varphi_\sigma}. \tag{29}$$

For energies close to the band gap energy of type I-spinors, $E \to 2\lambda$, scattering from the boundary acts as a spin polarizer since $\varphi'_\sigma \to \varphi_0 = \arctan(1/(2\sqrt{2})) \approx 19.5^\circ$ for all incoming spin directions φ_σ. This angle corresponds to $\langle\sigma_y\rangle = 1/3$. For $E = \lambda(2+\epsilon^2)$ with $\epsilon \ll 1$, we obtain

$$\varphi'_\sigma = \arctan\left(\frac{1}{2\sqrt{2}}\right) + \frac{2}{3}\epsilon\cos\varphi + \frac{\sqrt{2}}{72}\epsilon^2(\cos(2\varphi) - 5). \tag{30}$$

This is a surprising result since $R_1 \to -1$ and the incoming and reflected waves seem to compensate. But even though $R_2 \to -\sqrt{6}\epsilon e^{-i\varphi}\sin\varphi$ tends to zero, its admixture has a dominating effect.

For the upper boundary, we obtain the expansion

$$\varphi'_\sigma = \pi + \arctan\left(\frac{1}{2\sqrt{2}}\right) - \frac{2}{3}\epsilon\cos\varphi + \frac{\sqrt{2}}{72}\epsilon^2(\cos(2\varphi) - 5). \tag{31}$$

Note that the different sign compared to equation (30) results in a different asymptotic behavior for large energies since $\varphi'_\sigma(E = 2\lambda)$ is larger than the maximal incident spin direction $\varphi_\sigma = \pi$. This different behavior is illustrated on the right-hand side of figure 2.

3.1.2. Scattering behavior for plane waves of type II with $E \geqslant 2\lambda$. For a plane wave scattered at $y = 0$ with $A_1 = 0$ and $A_2 = 1$ with energy $E \geqslant 2\lambda$, the boundary conditions yield the following expressions for R_1, R_2:

$$R_1 = \mp z_1^2 \frac{(z_2 s_2 \pm c_2)^2 - (z_2 c_2 \pm s_2)^2 z_2^2}{(z_1 s_1 \pm c_1)(z_2 s_2 \pm c_2) z_1 + (z_1 c_1 \pm s_1)(z_2 c_2 \pm s_2) z_2}, \tag{32}$$

$$R_2 = \mp z_2^2 \frac{(z_1 c_1 \pm s_1)(z_2 s_2 \pm c_2) + (z_1 s_1 \pm c_1)(z_2 c_2 \pm s_2) z_1 z_2}{(z_1 s_1 \pm c_1)(z_2 s_2 \pm c_2) z_1 + (z_1 c_1 \pm s_1)(z_2 c_2 \pm s_2) z_2}. \tag{33}$$

For $(E - 2|\lambda|)/(E + 2|\lambda|) > (\cos\varphi)^2$, the abbreviations are the same as in equations (27) and (28). For $(E - 2|\lambda|)/(E + 2|\lambda|) < (\cos\varphi)^2$, the reflected momentum $k_y^1 = \pm iq$ is imaginary with

$$\hbar v_F q = \sqrt{-(E - |\lambda|)^2 + \lambda^2 + (\hbar v_F k_x)^2}. \tag{34}$$

The sign is determined to yield an exponential decay in the reflected region. In equations (32) and (33), z_1 is thus replaced by $z_1 \to (k_x \mp q)/\sqrt{k_x^2 - q^2}$, where the upper (lower) sign holds for reflections from the upper (lower) boundary, and s_1 by $s_1 \to i\sqrt{(\cos\vartheta_1 - 1)/2}$.

First let us discuss the scattering behavior from the lower boundary. On the left-hand side of figure 3, the reflected spin direction is plotted against the incident spin direction rotated by π. For large energies and normal incident direction $\varphi \approx \pi/2$, we again obtain $\varphi'_\sigma = \varphi_\sigma$. But for nearly parallel incident direction such that $(E - 2|\lambda|)/(E + 2|\lambda|) < (\cos\varphi)^2$, we obtain $\varphi'_\sigma = \pm\pi/2$. For energies close to the band-gap $E \to 2\lambda$, all reflected modes of type I are evanescent and scattering from the wall acts as a switch, which leads to either $\varphi'_\sigma = \pi/2$ or $\varphi'_\sigma = -\pi/2$.

It is understood that the appearance of the two extreme values of $\varphi'_\sigma = \pm\pi/2$ in the regime where k_y^1 is imaginary. Since z_1 is real and the incident and reflected waves of type $|\chi_{2,+}\rangle$ compensate, the expectation value in the x-direction $\langle\sigma_x\rangle = 0$. For the incident wave, $\langle|\sigma_y|\rangle_{\text{incident}}$ is negative, and for small incident angle, we thus have $\varphi'_\sigma = -\pi/2$. But if $|R_1|$ is large, the admixture of $|\chi_{1,+}\rangle$ can lead to $\varphi'_\sigma = \pi/2$. Additionally, the spin in the z-direction $\langle\sigma_z\rangle$ assumes a nonzero value to guarantee $|\langle\vec{\sigma}\rangle| = 1$. On the left-hand side of figure 4, this general behavior shows whether the reflected spin angle (rotated by π), the expectation values $\langle\sigma_i\rangle$ $(i = x, y, z)$ and the absolute value of the reflection amplitudes $|R_1|$ and $|R_2|$ are plotted versus the incident spin direction at $y = 0$ at energy $E = 3\lambda$.

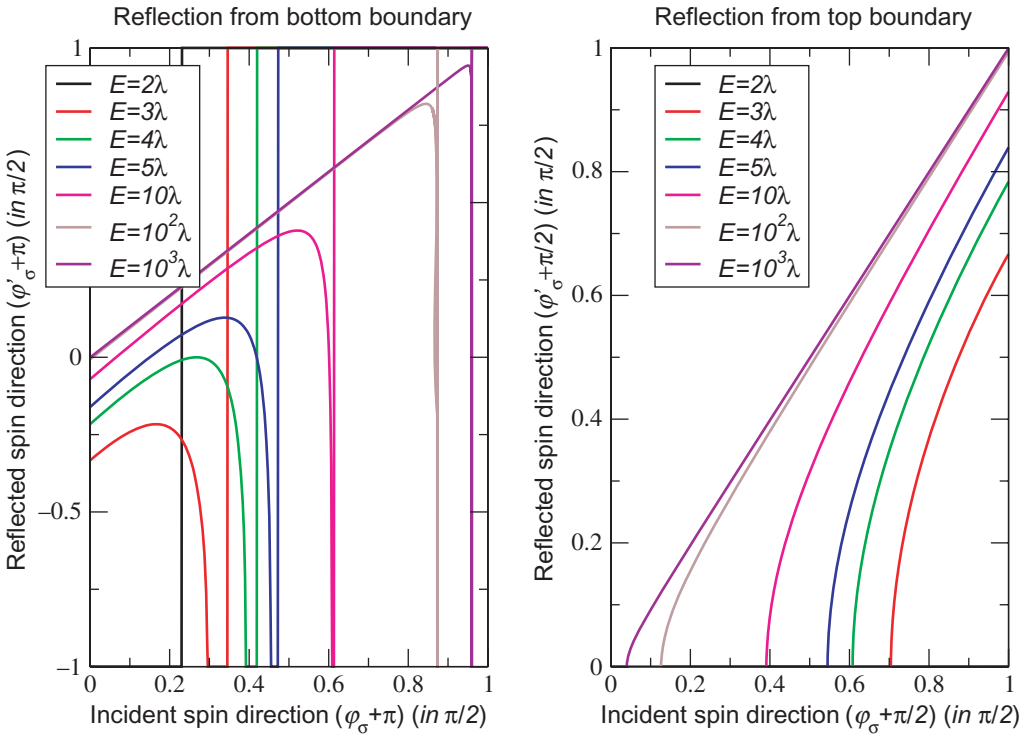

Figure 3. The reflected versus the incident spin direction (rotated by π) at $y = 0$ and $A_1 = 0$ for various energies $E \geqslant 2\lambda$. We use $\hbar v_F = 5.6\,\mathrm{eV\AA}$ and $\lambda = 6\,\mathrm{meV}$. Left: Reflection from the lower boundary. Right: Reflection from the upper boundary.

The scattering behavior from the upper boundary is considerably simpler. There, only two regimes appear, which are marked by whether k_y^1 is real or imaginary. This can be seen on the right-hand side of figures 3 and 4.

3.1.3. Scattering behavior for plane waves of type II with $E < 2\lambda$. For energies with $E < 2\lambda$, one of the reflected modes becomes evanescent, which leads to $\langle\sigma_x\rangle = 0$. For a more detailed analysis, we have to distinguish the two cases $E > \lambda$ and $E < \lambda$.

For $\lambda < E < 2\lambda$, the reflected momentum $k_y^1 = \pm \mathrm{i}q$ is imaginary with the same expression as in equation (34). The sign is determined to yield an exponential decay in the reflected region. With the ansatz

$$\psi_{E,k_x}(x, y) = \mathcal{N}_{\bar{k}} \mathrm{e}^{\mathrm{i}k_x x}\left[\mathrm{e}^{\mathrm{i}k_y^2 y}|\chi_{2,+}(k_x, k_y^2)\rangle + \widetilde{R}_1 \mathrm{e}^{-q|y|}|\chi_{1,+}(k_x, \pm \mathrm{i}q)\rangle + R_2 \mathrm{e}^{-\mathrm{i}k_y^2 y}|\chi_{2,+}(k_x, -k_y^2)\rangle\right], \tag{35}$$

we obtain the same expressions for $\widetilde{R}_1 \to R_1$ and R_2 as in equations (32) and (33) with the replacement $c_1 \to \sqrt{(1+\cos\vartheta_1)/2}$, $s_1 \to \mathrm{i}\sqrt{(\cos\vartheta_1 - 1)/2}$ and $z_1 \to -\mathrm{i}(k_x \mp q)/\sqrt{q^2 - k_x^2}$, where the upper (lower) sign holds for reflections from the upper (lower) boundary.

The lower boundary is to be discussed first. For small incident spin direction, $\langle\sigma_y\rangle > 0$ and becomes zero at $\varphi_\sigma = \varphi_E < \varphi_0 \approx 19.5^\circ$. The reflected spin angle is thus $\varphi'_\sigma = \pi/2$ for $\varphi > \varphi_E$ and $\varphi'_\sigma = -\pi/2$ for $\varphi < \varphi_E$ and for $E \to \lambda$ we have $\varphi_{E\to\lambda} = 0$.

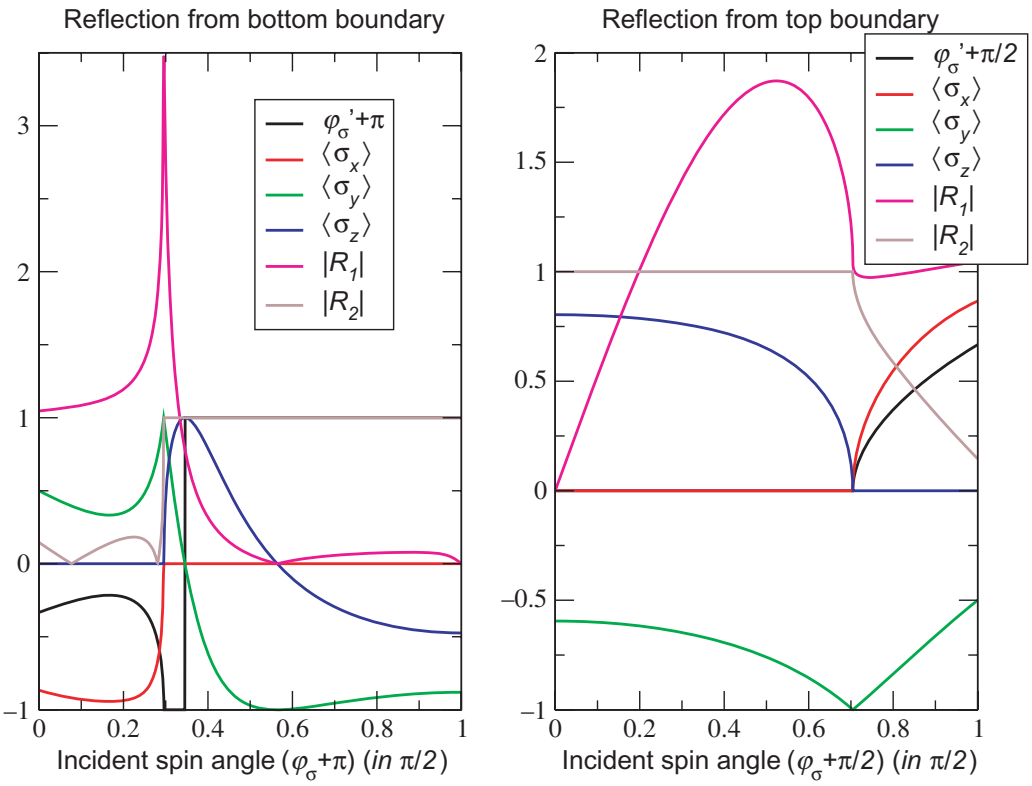

Figure 4. The reflected spin angle (rotated by π), the expectation values $\langle\sigma_i\rangle$ $(i = x, y, z)$ and the absolute value of the reflection amplitudes $|R_1|$ and $|R_2|$ versus the incident spin direction at $y = 0$ and $A_2 = 0$ for energies $E = 3\lambda$. We use $\hbar v_F = 5.6\,\mathrm{eV\AA}$ and $\lambda = 6\,\mathrm{meV}$. Left: Reflection from the lower boundary. Right: Reflection from the upper boundary.

For the upper boundary, we have $\langle\sigma_y\rangle < 0$ for all angles and energies. In both cases, we have $\langle\sigma_z\rangle \neq 0$ to fulfill the sum rule $|\langle\vec{\sigma}\rangle| = 1$.

For energies with $0 < E < \lambda$, there is no reflected wave of type I, $|\chi_{1,+}\rangle$, but one of the reflected momenta of $|\chi_{2,+}\rangle$ is imaginary, $k_y^2 = \pm iq$ with the same definition as in equation (34). With

$$\psi_{E,k_x}(x, y) = \mathcal{N}_{\tilde{k}} e^{ik_x x}\left[e^{ik_y^2 y}|\chi_{2,+}(k_x, k_y^2) + \widetilde{R}_2 e^{-q|y|}|\chi_{2,+}(k_x, \pm iq)\rangle + R_2 e^{-ik_y^2 y}|\chi_{2,+}(k_x, -k_y^2)\rangle\right], \tag{36}$$

we have

$$\widetilde{R}_2 = \mp\tilde{z}_2^2 \frac{(z_2 s_2 \pm c_2)^2 - (z_2 c_2 \pm s_2)^2 z_2^2}{(\tilde{z}_2\tilde{s}_2 \pm \tilde{c}_2)(z_2 c_2 \pm s_2)z_2 - (\tilde{z}_2\tilde{c}_2 \pm \tilde{s}_2)(z_2 s_2 \pm c_2)\tilde{z}_2}, \tag{37}$$

$$R_2 = \mp z_2^2 \frac{(\tilde{z}_2\tilde{s}_2 \pm \tilde{c}_2)(z_2 s_2 \pm c_2) - (\tilde{z}_2\tilde{c}_2 \pm \tilde{s}_2)(z_2 c_2 \pm s_2)\tilde{z}_2 z_2}{(\tilde{z}_2\tilde{s}_2 \pm \tilde{c}_2)(z_2 c_2 \pm s_2)z_2 - (\tilde{z}_2\tilde{c}_2 \pm \tilde{s}_2)(z_2 s_2 \pm c_2)\tilde{z}_2}, \tag{38}$$

with $\tilde{c}_2 = \sqrt{(1 + \cos\vartheta_2^e)/2}$, $\tilde{s}_2 = i\sqrt{(\cos\vartheta_2^e - 1)/2}$, $\tilde{z}_2 = -i(k_x \mp q)/\sqrt{q^2 - k_x^2}$ and $\vartheta_2^e = |\lambda|/(|\lambda| - E)$. In the above equations, the upper (lower) sign holds for reflections from the upper (lower) boundary.

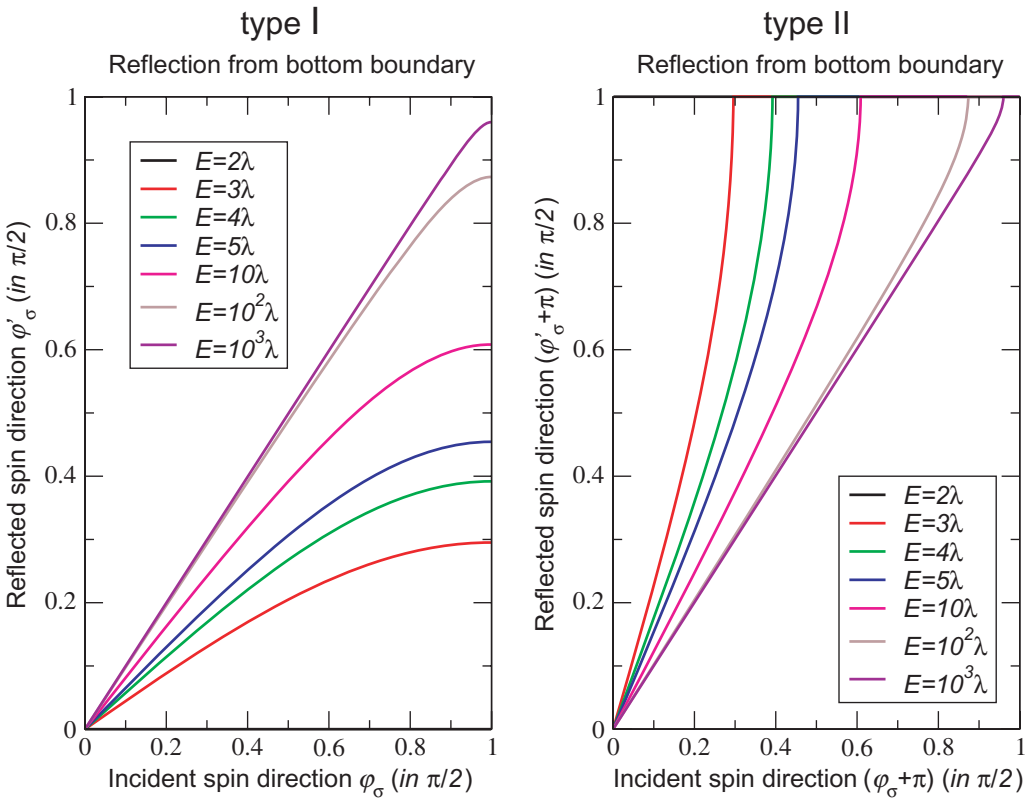

Figure 5. The reflected versus the incident spin direction at $y = 0$ with $A_2 = 0$ (left-hand side) and $A_1 = 0$ (rotated by π) (right-hand side) for various energies $E \geqslant 2\lambda$ in the case of a zigzag boundary. We use $\hbar v_F = 5.6\,\text{eV\AA}$ and $\lambda = 6\,\text{meV}$.

We obtain $\langle \sigma_y \rangle = -1$ for the upper and $\langle \sigma_y \rangle = 1$ for the lower boundary, respectively, which is independent of the incident direction and the energy.

3.2. Zigzag boundary

Graphene can be terminated by a zigzag boundary that exposes only one sublattice to the boundary. With $\psi_{E,k_x} = (\psi_1, \psi_2, \psi_3, \psi_4)^{\mathrm{T}}$, the boundary conditions at a zigzag boundary thus read

$$\psi_1 = \psi_2 = 0 \quad \text{(for bottom boundary)}, \qquad \psi_3 = \psi_4 = 0 \quad \text{(for top boundary)}. \tag{39}$$

Here, we assumed that the bottom boundary is terminated by sublattice A and the top boundary by sublattice B.

For a general plane wave equation (23) scattered at $y = 0$ with energy $E \geqslant 2\lambda$, the boundary conditions for the bottom boundary (sublattice A) equation (39) yield the following expressions for R_1, R_2:

$$R_1 = -z_1^2 \frac{A_1(s_1 s_2 + c_1 c_2 z_1 z_2) + A_2(s_2 c_2 - s_2 c_2 z_2^2)}{s_1 s_2 z_1^2 + c_1 c_2 z_1 z_2}, \tag{40}$$

$$R_2 = -z_2^2 \frac{A_1(s_1 c_1 - s_1 c_1 z_1^2) + A_2(c_1 c_2 + s_1 s_2 z_1 z_2)}{c_1 c_2 z_2^2 + s_1 s_2 z_1 z_2}. \tag{41}$$

The boundary conditions for the upper boundary (sublattice B) yield the following expressions for R_1, R_2:

$$R_1 = -z_1^2 \frac{A_1 z_1 (c_1 c_2 + s_1 s_2 z_1 z_2) + A_2 z_2 (s_2 c_2 - s_2 c_2 z_2^2)}{c_1 c_2 z_1 + s_1 s_2 z_2}, \tag{42}$$

$$R_2 = -z_2^2 \frac{A_1 z_1 (s_1 c_1 - s_1 c_1 z_1^2) + A_2 z_2 (s_1 s_2 + c_1 c_2 z_1 z_2)}{c_1 c_2 z_1 + s_1 s_2 z_2}. \tag{43}$$

The abbreviations are the same as for the infinite mass boundary. Since the reflected angle is symmetric around normal incidence, we will only discuss reflection from the bottom boundary for $k_x > 0$.

In figure 5, the reflected versus the incident spin direction at $y = 0$ is shown for the two types of incident plane waves. As in the case of the infinite mass boundary, $\langle \sigma_x \rangle = 0$ for incident plane waves of type II with $\cos^2 \varphi > (E - 2|\lambda|)/(E + 2|\lambda|)$. But contrary to the infinity mass boundary, the spin polarization in the out-of-plane direction assumes a nonzero value even when the reflected wave of type I is extended. For this case, i.e. $k_y^1 \in \mathbf{R}$, we obtain

$$\langle \sigma_z \rangle^{\mathrm{I}} = -\frac{|\lambda|}{E + |\lambda|}, \quad \langle \sigma_z \rangle^{\mathrm{II}} = \frac{|\lambda|}{E - |\lambda|}. \tag{44}$$

The K'-point yields the opposite sign so that there is no net polarization in the z-direction. For energies $E < 2\lambda$, a similar discussion as in the case of infinite mass boundary applies.

4. Spin polarization close to the boundary

So far we have only discussed polarization properties at the boundary $y = 0$. For finite y, we expect an oscillatory behavior of the reflected spin polarization. For $E \to 2\lambda$ and plane wave scattering of type I, $k_y^1 \to 0$ and the period will thus be solely determined by $k_y^2 \to \sqrt{2}(2\lambda/\hbar v_F)$. This oscillatory behavior is again independent of incident spin polarization and results in a striped phase for the reflected spin polarization. For $E > 2\lambda$, two periods related to $k_y^{1/2}$ contribute and a more complicated pattern emerges, which also depends on the incident spin polarization and whether one deals with a reflection from the top or from the bottom. This hints to the fact that a Dirac particle in a box shows quasi-chaotic behavior [29].

In the following, we will study the spin polarization averaged over the incident direction for fixed A_1, A_2 and including the two K-points as a function of the y-direction. We will further average over positive and negative k_x momenta. With an incident wave of type μ and momentum $k^\mu = \sqrt{(E + (-1)^\mu |\lambda|)^2 - \lambda^2}/(\hbar v_F)$, $\mu \in \{1, 2\}$, we have

$$\langle \vec{\rho} \rangle^\mu (\vec{r}) \equiv \frac{1}{2} \sum_{\kappa = K, K'} \frac{1}{\pi} \int_0^\pi \mathrm{d}\varphi \langle \psi_{E, k^\mu \cos\varphi} | \vec{\sigma} \delta(\vec{r} - \hat{\vec{r}}) | \psi_{E, k^\mu \cos\varphi} \rangle_\kappa. \tag{45}$$

We only discuss the spin polarization at the lower boundary, which depends on the sign of λ (here we choose $\lambda = |\lambda|$). The spin polarization on the upper boundary is obtained by reversing the sign.

In figure 6, the angle-averaged spin density $\mathcal{A}\langle \rho_x \rangle^\mu (\vec{r})$ is shown as a function of y for various energies $E \geqslant 2\lambda$, where $\mathcal{A}$ denotes the area of the sample. We show the results for an incident plane wave of type I (left-hand side) and type II (right-hand side) with an infinite mass

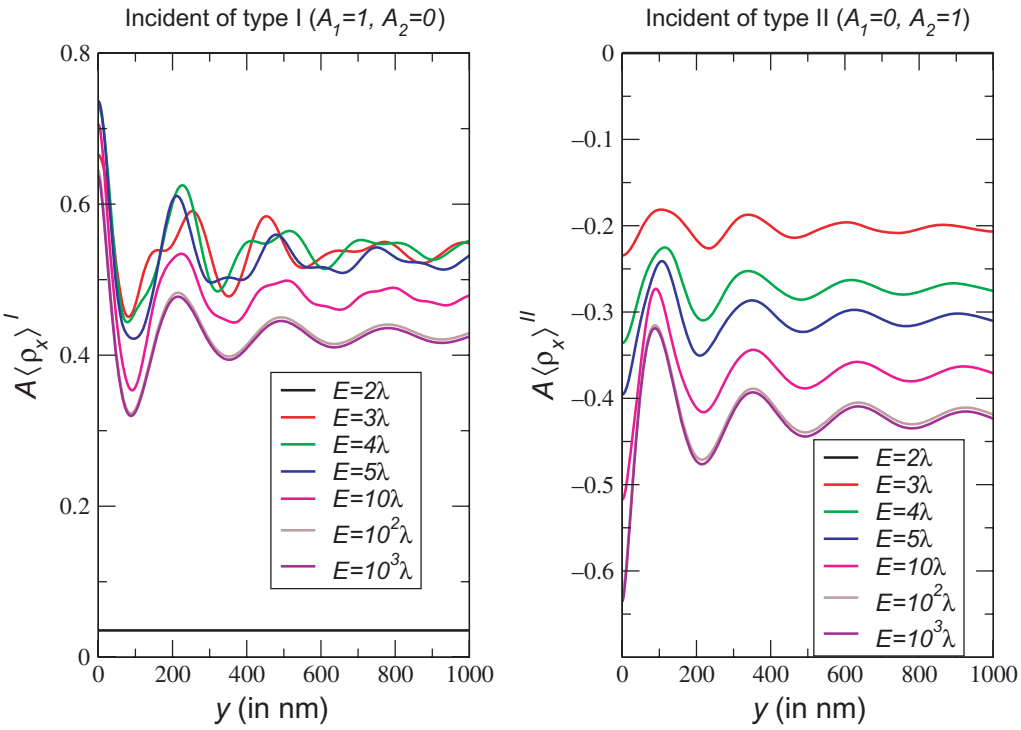

Figure 6. Spin polarization in the x-direction as a function of y for various energies $E \geqslant 2\lambda$ with an infinite mass boundary. We use $\hbar v_F = 5.6\,\mathrm{eV\AA}$ and $\lambda = 6\,\mathrm{meV}$. Left: Incident plane wave of type I. Right: Incident plane wave of type II.

boundary. There is a clear difference between the two types for low energies, which is due to the appearance of imaginary momenta $k_y^1 = \pm \mathrm{i}q$ for type II reflections. For low energies, most incident angles of the initial plane wave of type II lead to evanescent modes and thus to $\langle\sigma_x\rangle = 0$. For large energies $E \geqslant 10^3\lambda$, the spin polarizations of the two types have approximately the same absolute value, but differ in sign.

Obviously, the above ensemble average breaks time-reversal symmetry since there is one incident plane wave with fixed k_y-direction and two reflected plane waves. But if there is no coherence between the incident plane waves of types I and II, e.g. due to temperature, then time-reversal symmetry is effectively broken and we find a net polarization in the x-direction by adding the two contributions $\langle\vec{\rho}\rangle^{\mathrm{I}}$ and $\langle\vec{\rho}\rangle^{\mathrm{II}}$ (and possibly weighting them with the corresponding density of states). This is demonstrated in figure 7, where the sum of the two contributions $\mathcal{A}\sum_\mu\langle\vec{\rho}\rangle^\mu$ is shown for an infinite mass boundary (left) and for a zigzag boundary (right). Moreover, we expect spin polarization in the x-direction for various non-equilibrium situations.

In the other two directions, we find no net spin polarization if the two inequivalent K-points are included. We note, however, that ρ_y and ρ_z assume a finite value for one K-point, only. This opens up the possibility of spin polarization in these directions in the presence of ripples or a magnetic field. Especially surface states due to e.g. zigzag boundaries that effectively break the sublattice symmetry and that are not included in our continuous model should give rise to a finite spin polarization.

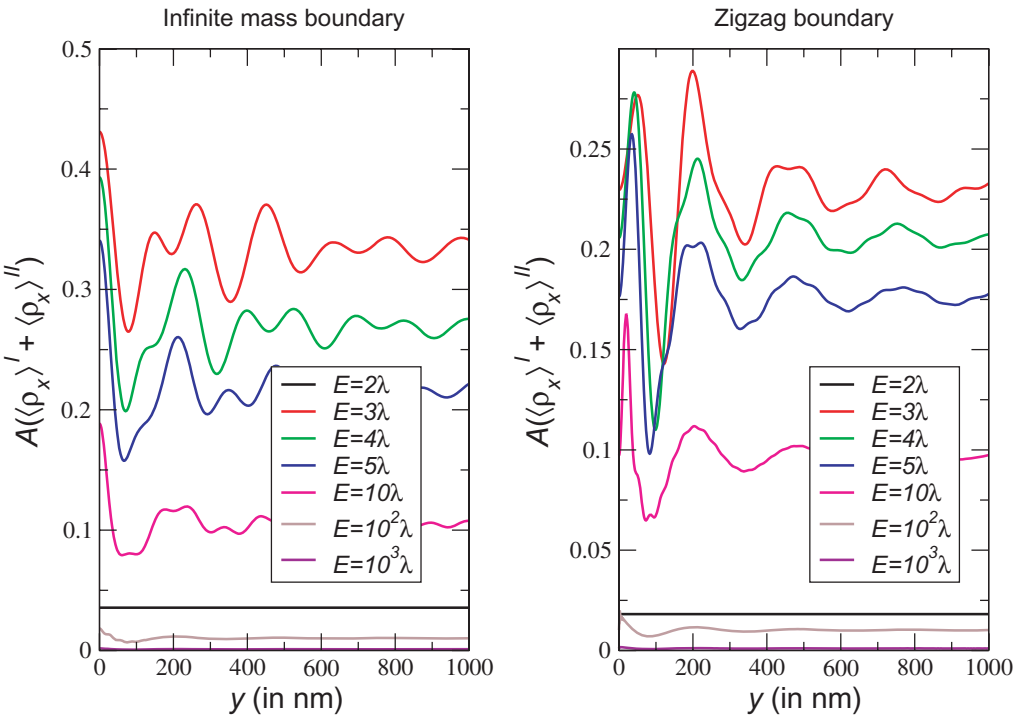

Figure 7. Net spin polarization in the x-direction as a function of y for various energies $E \geqslant 2\lambda$. We use $\hbar v_F = 5.6\,\mathrm{eV\AA}$ and $\lambda = 6\,\mathrm{meV}$. Left: Infinite mass boundary. Right: Zigzag boundary.

5. Dirac electrons with 'pseudo-Rashba' spin–orbit coupling in nanoribbons

In this section, we will consider graphene nanoribbons and the quantization properties of transverse momenta in the presence of 'pseudo-Rashba' spin–orbit coupling. We will then discuss the density and spin distribution at various energies.

5.1. Quantization of the transverse momentum

First the infinite mass boundaries are considered. For a general plane wave with fixed momentum k_x and energy E, $\psi_{E,k_x}(x, y) \equiv (\psi_1, \psi_2, \psi_3, \psi_4)^{\mathrm{T}}$, there are four conditions that have to be satisfied, i.e. $\psi_1 = \pm\psi_3$ and $\psi_2 = \pm\psi_4$ at $y = 0$, and $\psi_1 = \mp\psi_3$ and $\psi_2 = \mp\psi_4$ at $y = W$, where the upper (lower) sign stands for the K (K')-point and W is the width of the nanoribbon. For a zigzag nanoribbon that terminates on sublattice A at the bottom and on sublattice B at the top, the four conditions read as $\psi_1 = \psi_2 = 0$ at $y = 0$ and $\psi_3 = \psi_4 = 0$ at $y = W$.

Let us first assume two propagating waves as in equation (23), see also figure 8. In order to have a nontrivial solution, a necessary condition is

$$\det M = \det \begin{pmatrix} A & \bar{A} \\ B & \bar{B} \end{pmatrix} = \det \left(A B^{-1} - \bar{A} \bar{B}^{-1} \right) \det B \det \bar{B} = 0, \tag{46}$$

with the bar denoting the complex conjugate.

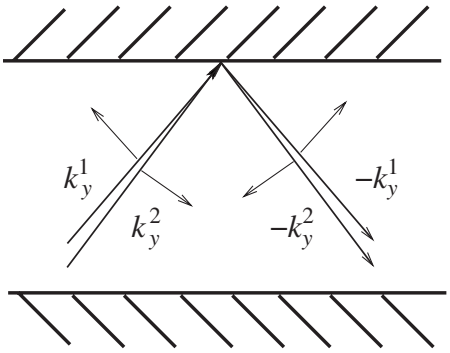

Figure 8. A superposition of plane waves of type I and type II with constant k_x reflected at one boundary of a nanoribbon into another superposition of plane waves of type I and type II.

For infinite mass boundaries, the above matrices read at the K-point

$$A = \begin{pmatrix} s_1 - c_1 z_1 & c_2 - s_2 z_2 \\ (c_1 - s_1 z_1) z_1 & (-s_2 + c_2 z_2) z_2 \end{pmatrix}, \quad B = \begin{pmatrix} (s_1 + c_1 z_1) w_1 & (c_2 + s_2 z_2) w_2 \\ (c_1 + s_1 z_1) z_1 w_1 & -(s_2 + c_2 z_2) z_2 w_2 \end{pmatrix}, \tag{47}$$

and for zigzag boundaries, we have

$$A = \begin{pmatrix} s_1 & c_2 \\ c_1 z_1 & -s_2 z_2 \end{pmatrix}, \quad B = \begin{pmatrix} c_1 z_1 w_1 & s_2 z_2 w_2 \\ s_1 z_1^2 w_1 & -c_2 z_2^2 w_2 \end{pmatrix}, \tag{48}$$

where we introduced $w_\mu = \mathrm{e}^{\mathrm{i}k_y{}^\mu W}$ and used the definitions of section 3. $\det M$ in equation (46) is real and thus yields quantization of the transverse momentum in the y-direction.

For $(\hbar v_F k_y^2)^2 < 4E\lambda$, there is the appearance of evanescent modes since $k_y^1 = \pm \mathrm{i}q$ is imaginary. In this case, a general plane wave with fixed momentum k_x and energy $E \geqslant 2|\lambda|$, $\psi_{E,k_x}(x, y) \equiv (\psi_1, \psi_2, \psi_3, \psi_4)^{\mathrm{T}}$, is written as

$$\begin{aligned} \psi_{E,k_x}(x, y) = \mathcal{N}_{\bar{k}} \mathrm{e}^{\mathrm{i}k_x x} \Big[& A_1 \mathrm{e}^{-q(W-y)} |\chi_{1,+}(k_x, -\mathrm{i}q)\rangle + A_2 \mathrm{e}^{\mathrm{i}k_y^2 y} |\chi_{2,+}(k_x, k_y^2)\rangle \\ & + R_1 \mathrm{e}^{-qy} |\chi_{1,+}(k_x, \mathrm{i}q)\rangle + R_2 \mathrm{e}^{-\mathrm{i}k_y^2 y} |\chi_{2,+}(k_x, -k_y^2)\rangle \Big], \end{aligned} \tag{49}$$

with

$$\hbar v_F q = \sqrt{-(E - |\lambda|)^2 + \lambda^2 + (\hbar v k_x)^2}, \quad \hbar v_F k_y^2 = \sqrt{(E + |\lambda|)^2 - \lambda^2 - (\hbar v k_x)^2}. \tag{50}$$

Again, in order to have a nontrivial solution, equation (46) must hold, but this time the matrices for infinite mass boundaries at the K-point read

$$A = \begin{pmatrix} (s_1 - c_1 z_1^+) w_1 & c_2 - s_2 z_2 \\ (c_1 - s_1 z_1^+) z_1^+ w_1 & (-s_2 + c_2 z_2) z_2 \end{pmatrix}, \quad B = \begin{pmatrix} s_1 + c_1 z_1^+ & (c_2 + s_2 z_2) w_2 \\ (c_1 + s_1 z_1^+) z_1^+ & -(s_2 + c_2 z_2) z_2 w_2 \end{pmatrix}, \tag{51}$$

and for zigzag boundaries, we have

$$A = \begin{pmatrix} s_1 w_1 & c_2 \\ c_1 z_1^+ w_1 & -s_2 z_2 \end{pmatrix}, \quad B = \begin{pmatrix} c_1 z_1^+ & -s_2 z_2 w_2 \\ s_1 (z_1^+)^2 & -c_2 z_2^2 w_2 \end{pmatrix}, \tag{52}$$

with $w_1 = \mathrm{e}^{-qW}$, $z_1^{\pm} = (k_x \pm q)/\sqrt{k_x^2 - q^2}$, $c_1 \to \sqrt{(1+\cos\vartheta_1)/2}$ and $s_1 \to \mathrm{i}\sqrt{(\cos\vartheta_1 - 1)/2}$. The definitions for the plane wave of type II remain unchanged. Since the wave function of the evanecent mode is now real, matrices $\bar{A}$, $\bar{B}$ are not the complex conjugates of A, B, but given by

$$\bar{A} = \begin{pmatrix} s_1 - c_1 z_1^- & c_2 - s_2 z_2^* \\ (c_1 - s_1 z_1^-) z_1^- & (-s_2 + c_2 z_2^*) z_2^* \end{pmatrix}, \quad \bar{B} = \begin{pmatrix} (s_1 + c_1 z_1^-) w_1 & (c_2 + s_2 z_2^*) w_2^* \\ (c_1 + s_1 z_1^-) z_1^- w_1 & -(s_2 + c_2 z_2^*)(z_2 w_2)^* \end{pmatrix}, \tag{53}$$

for infinite mass boundaries, and for zigzag boundaries they read

$$\bar{A} = \begin{pmatrix} s_1 & c_2 \\ c_1 z_1^- & -s_2 z_2^* \end{pmatrix}, \quad \bar{B} = \begin{pmatrix} c_1 z_1^- w_1 & -s_2 (z_2 w_2)^* \\ s_1 (z_1^-)^2 w_1 & -c_2 (z_2^2 w_2)^* \end{pmatrix}. \tag{54}$$

It is now preferable to write equation (46) in powers of w_1. For zigzag boundaries, this yields

$$\begin{aligned} \det M = {} & 2\mathrm{i}\,\mathrm{Im}\left(\det B \det \bar{A}\right) + 2w_1 (z_1^+ - z_1^-)(z_2 - \bar{z}_2) s_1 c_1 s_2 c_2 \\ & - w_1^2 \Big[z_1^- (w_2 z_2 - \bar{w}_2 \bar{z}_2) s_1 c_1 s_2 c_2 + (z_1^-)^2 (w_2 - \bar{w}_2) s_1^2 s_2^2 + (w_2 z_2 - \bar{w}_2 \bar{z}_2) c_1^2 c_2^2 \Big] = 0, \end{aligned} \tag{55}$$

which is purely imaginary and thus again yields quantization of the transverse momentum in the y-direction. For infinite mass boundaries, we obtain a similar expression.

5.2. *Spin and density distribution*

The particle density $\langle n \rangle$ at energy E is now obtained by summing over all transverse modes n that obey the above boundary conditions or the corresponding boundary conditions for the K'-point. Denoting the nth transverse momentum of type II by $k_{y,n}^2$, we have

$$\langle n \rangle (\vec{r}) = \sum_n \sum_{k_x} \langle \psi_{E,k_x} | \delta(\vec{r} - \hat{\vec{r}}) | \psi_{E,k_x} \rangle \delta_{E, E_{k_x, k_{y,n}^2}}. \tag{56}$$

In figure 9, the density distribution of a graphene nanoribbon of width $W = 100\,\mathrm{nm}$ for various low energies with infinite mass (left) and zigzag (right) boundaries is shown. In general, the number of modes is the same with and without 'pseudo-Rashba' spin–orbit coupling and the resulting density distributions only differ slightly. But for zigzag boundaries at $E = 4\lambda$, we observe strong deviations due to the fact that there are eight modes in the case with spin–orbit coupling in contrast to 12 modes in the case without spin–orbit coupling. Also note that whereas for the case without spin–orbit coupling all modes are extended, some modes for the case with spin–orbit coupling are evanescent for the type I branch. For zigzag boundaries e.g. we have no extended and four evanescent (type-I) modes at $E = 2\lambda$, six extended and two evanescent modes at $E = 4\lambda$, and six extended and six evanescent modes at $E = 6\lambda$.

The spin polarization at the boundaries is in all cases zero; in the x-direction it is zero also for only one K-point, in the y- and z-directions it is nonzero for one K-point, but averages to zero when two K-points are included. This is an immediate consequence of time-reversal symmetry. In [30], spin polarization in the z-direction is reported for various k_x-values within a lattice model of a zigzag nanoribbon. At equilibrium, this can only be attributed to edge states that effectively break the sublattice symmetry and that are not included in our continuous model.

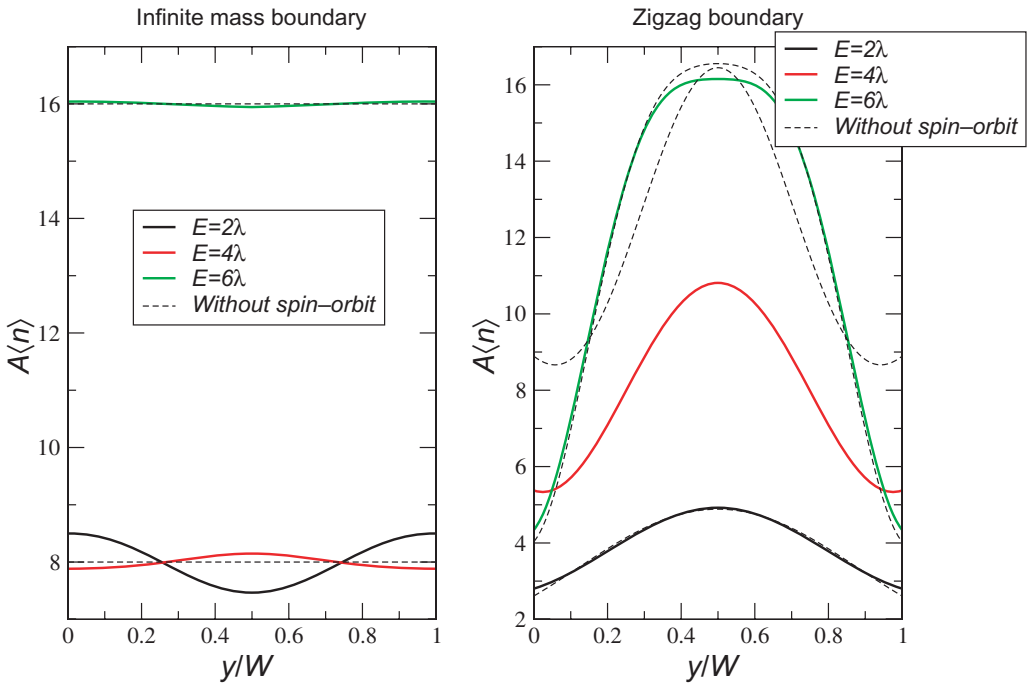

Figure 9. The density distribution of a graphene nanoribbon of width $W = 100\,\text{nm}$ for various low energies. We use $\hbar v_F = 5.6\,\text{eV\AA}$ and $\lambda = 6\,\text{meV}$. Left-hand side: Infinite mass boundaries. Right-hand side: Zigzag boundaries. The corresponding density distributions without 'pseudo-Rashba' spin–orbit coupling are also shown (dashed lines).

6. Summary

In this paper, we have investigated the spin dephasing of Dirac fermions with 'pseudo-Rashba' spin–orbit coupling due to reflection from a hard wall. In order to confine the Dirac electrons, we used infinite mass and zigzag boundaries. For large energies compared to the spin–orbit coupling, we obtained the expected result that there is hardly spin dephasing due to the scattering process. But for energies close to the band gap for plane waves of type I, $E \approx 2\lambda$, strong spin dephasing is observed. If the incident plane wave is of type II (gapless branch), even stronger effects are seen like the appearance of evanescent modes. We also observe rotation of the spin in the out-of-plane direction away from the boundary and for incident plane waves of type II also at the boundary. This effect will be cancelled by averaging over the two inequivalent K-points.

We also discussed the spin polarization averaged over the incident direction and including the two K-points. We find that for energies $E \geqslant 2\lambda$, there is a finite spin polarization in the x-direction when there is no coherence between the two branches. This polarization differs in sign for the upper and lower boundary, respectively. Also for non-equilibrium situations, there will be a spin polarization in this direction.

We finally analyzed the spin and density distribution of graphene nanoribbons. At certain energies, the number of transverse modes does not match that of a corresponding nanoribbon without 'pseudo-Rashba' spin–orbit coupling. This results in significant changes in the density distribution. But generally, the 'pseudo-Rashba' spin–orbit coupling leads to

marginal differences, only. Further, there is no spin polarization if both K-points are included, but we find a finite spin polarization in the y- and z-directions for one K-point, only. Surface states due to e.g. zigzag boundaries, which only live on one sublattice and thus break the valley symmetry, should therefore yield a finite spin polarization.

Acknowledgments

TS wants to thank Nuno Peres and João Lopes dos Santos for illuminating discussions and support. We further thank E Rashba for useful comments on the manuscript. This work was funded by FCT via projects PTDC/FIS/64404/2006, PTDC/FIS/101434/2008 and by Deutsche Forschungsgemeinschaft via SFB 689.

Appendix A. The full model including the two K-points

The full model including the two K-points reads as

$$H = v\left(p_x\kappa_z\tau_x + p_y\tau_y\right) + \lambda\left(\kappa_z\tau_x\sigma_y - \tau_y\sigma_x\right), \tag{57}$$

where $\kappa_z = \pm 1$ denotes the two inequivalent K-points. For a given wave vector $\vec{k}$, the Hamiltonian around the K'-point ($\kappa_z = -1$) reads as

$$\mathcal{H}(\vec{k}) = -\begin{pmatrix} 0 & 0 & \hbar v_F(k_x + \mathrm{i}k_y) & -2i\lambda \\ 0 & 0 & 0 & \hbar v_F(k_x + \mathrm{i}k_y) \\ \hbar v_F(k_x - \mathrm{i}k_y) & 0 & 0 & 0 \\ 2i\lambda & \hbar v_F(k_x - \mathrm{i}k_y) & 0 & 0 \end{pmatrix}. \tag{58}$$

The Hamiltonian around the K'-point can thus be obtained from the Hamiltonian around the K-point by interchanging the pseudo-spin index and reversing the sign. All previous results without the mass term can thus be used. The results involving the mass term are obtained by $M \to -M$. This leads to a change in the boundary conditions, i.e.

$$\left.\frac{\psi_1}{\psi_3}\right|_{\text{bottom}}^{K'} = \left.\frac{\psi_2}{\psi_4}\right|_{\text{bottom}}^{K'} = -1, \quad \left.\frac{\psi_1}{\psi_3}\right|_{\text{top}}^{K'} = \left.\frac{\psi_2}{\psi_4}\right|_{\text{top}}^{K'} = 1. \tag{59}$$

Appendix B. Massive Dirac fermions with 'pseudo-Rashba' spin–orbit coupling

Massive Dirac fermions with 'pseudo-Rashba' spin–orbit interaction can be described by

$$\mathcal{H} = v\vec{p}\cdot\vec{\tau} + \lambda\left(\vec{\tau}\times\vec{\sigma}\right)\cdot\vec{e}_z + Mv^2\tau_z, \tag{60}$$

where, among standard notation, λ is the spin–orbit coupling parameter, and the Pauli matrices $\vec{\tau}$, $\vec{\sigma}$ describe the sublattice and the electron spin degree of freedom, respectively.

Squaring the Hamiltonian, we obtain the same eigenvectors as for massless Dirac fermions given in equations (5) and (6). In the basis $(|\alpha_1\rangle, |\beta_1\rangle, |\alpha_2\rangle, |\beta_2\rangle)$, the Hamiltonian reads

$$\tilde{\mathcal{H}}(\vec{k}) = \begin{pmatrix} m & q_+^* & 0 & 0 \\ q_+ & -m & 0 & 0 \\ 0 & 0 & m & q_- \\ 0 & 0 & q_-^* & -m \end{pmatrix} \tag{61}$$

with

$$q_\pm = \pm\hbar v_F(k_x \pm \mathrm{i}k_y)\, f_\pm(|\lambda|/\hbar v_F k), \qquad m = Mv^2 \tag{62}$$

and

$$f_\pm(x) = \sqrt{1+x^2} \pm x. \tag{63}$$

Again we find two types of solutions. The first type has eigenvalues

$$\varepsilon_{1,\pm} = \pm\sqrt{M^2v^4 + (\hbar v_F k)^2 + 2\lambda^2 + 2|\lambda|\sqrt{(\hbar v_F k)^2 + \lambda^2}} \tag{64}$$

with eigenspinors

$$|\chi_{1,+}(\vec{k})\rangle = \begin{pmatrix} \sin(\vartheta/2)\cos(\zeta_1/2) \\ \cos(\vartheta/2)\cos(\zeta_1/2)\mathrm{e}^{\mathrm{i}\eta} \\ \cos(\vartheta/2)\sin(\zeta_1/2)\mathrm{e}^{\mathrm{i}\psi} \\ \sin(\vartheta/2)\sin(\zeta_1/2)\mathrm{e}^{\mathrm{i}\eta}\mathrm{e}^{\mathrm{i}\psi} \end{pmatrix}, \quad |\chi_{1,-}(\vec{k})\rangle = \begin{pmatrix} \sin(\vartheta/2)\sin(\zeta_1/2) \\ \cos(\vartheta/2)\sin(\zeta_1/2)\mathrm{e}^{\mathrm{i}\eta} \\ -\cos(\vartheta/2)\cos(\zeta_1/2)\mathrm{e}^{\mathrm{i}\psi} \\ -\sin(\vartheta/2)\cos(\zeta_1/2)\mathrm{e}^{\mathrm{i}\eta}\mathrm{e}^{\mathrm{i}\psi} \end{pmatrix} \tag{65}$$

with $\zeta_{1/2} \in [0, \pi]$ and

$$\cos\zeta_{1/2} = \frac{Mv^2}{\sqrt{|q_\pm|^2 + M^2v^4}}, \quad \mathrm{e}^{\mathrm{i}\psi} = \frac{k_x + \mathrm{i}k_y}{k}. \tag{66}$$

The second type has eigenvalues

$$\varepsilon_{2,\pm} = \pm\sqrt{M^2v^4 + (\hbar v_F k)^2 + 2\lambda^2 - 2|\lambda|\sqrt{(\hbar v_F k)^2 + \lambda^2}} \tag{67}$$

with eigenspinors

$$|\chi_{2,+}(\vec{k})\rangle = \begin{pmatrix} \cos(\vartheta/2)\cos(\zeta_2/2) \\ -\sin(\vartheta/2)\cos(\zeta_2/2)\mathrm{e}^{\mathrm{i}\eta} \\ \sin(\vartheta/2)\sin(\zeta_2/2)\mathrm{e}^{\mathrm{i}\psi} \\ -\cos(\vartheta/2)\sin(\zeta_2/2)\mathrm{e}^{\mathrm{i}\eta}\mathrm{e}^{\mathrm{i}\psi} \end{pmatrix}, \quad |\chi_{2,-}(\vec{k})\rangle = \begin{pmatrix} \cos(\vartheta/2)\sin(\zeta_2/2) \\ -\sin(\vartheta/2)\sin(\zeta_2/2)\mathrm{e}^{\mathrm{i}\eta} \\ -\sin(\vartheta/2)\cos(\zeta_2/2)\mathrm{e}^{\mathrm{i}\psi} \\ \cos(\vartheta/2)\cos(\zeta_2/2)\mathrm{e}^{\mathrm{i}\eta}\mathrm{e}^{\mathrm{i}\psi} \end{pmatrix}. \tag{68}$$

Let us now consider expectation values within the eigenstates with wave functions

$$\langle\vec{r}|\vec{k}, \mu, \pm\rangle = \frac{\mathrm{e}^{\mathrm{i}\vec{k}\vec{r}}}{\sqrt{\mathcal{A}}}|\chi_{\mu,\pm}\rangle, \tag{69}$$

$\mu \in \{1, 2\}$ and $\mathcal{A}$ being the area of the system. Here we find

$$\langle\vec{k}, \mu, \pm|\vec{\tau}|\vec{k}, \mu, \pm\rangle = \pm\begin{pmatrix} \sin\vartheta\,\sin\zeta_\mu\cos\varphi \\ \sin\vartheta\,\sin\zeta_\mu\sin\varphi \\ \cos\zeta_\mu \end{pmatrix} \tag{70}$$

and

$$\langle\vec{k}, 1, \pm|\vec{\sigma}|\vec{k}, 1, \pm\rangle = -\langle\vec{k}, 2, \pm|\vec{\sigma}|\vec{k}, 2, \pm\rangle = \begin{pmatrix} -\sin\vartheta\,\sin\varphi \\ \sin\vartheta\,\cos\varphi \\ \mp\cos\vartheta\,\cos\zeta_{1/2} \end{pmatrix}. \tag{71}$$

Here we have assumed a positive spin–orbit coupling parameter, $\lambda = |\lambda|$, and φ is the usual azimuthal angle of the wave vector, $\vec{k} = k(\cos\varphi, \sin\varphi)$. Note that massive Dirac fermions assume a nonzero expectation value for the pseudo-spin and spin in the z-direction.

Appendix C. Scattering from infinite mass boundary

Dirac fermions can be confined by an infinite mass boundary, first discussed by Berry and Mondragon [27]. In the following, we will study the scattering behavior from a boundary located at $y = 0$ and W. Within the strip $0 < y < W$, the mass of the Dirac fermions shall be zero; outside the strip, the mass shall be infinite.

A general plane wave within the strip with fixed momentum k_x and energy $E > 0$ can be written as

$$\psi_{E,k_x}(x, y) = \mathrm{e}^{\mathrm{i}k_x x}\Big[A_1\mathrm{e}^{\mathrm{i}k_y^1 y}|\chi_{1,+}(k_x, k_y^1)\rangle + A_2\mathrm{e}^{\mathrm{i}k_y^2 y}|\chi_{2,+}(k_x, k_y^2)\rangle + R_1\mathrm{e}^{-\mathrm{i}k_y^1 y}|\chi_{1,+}(k_x, -k_y^1)\rangle + R_2\mathrm{e}^{-\mathrm{i}k_y^2 y}|\chi_{2,+}(k_x, -k_y^2)\rangle\Big], \tag{72}$$

with

$$\hbar v_F k_y^\mu = \sqrt{(E + (-1)^\mu|\lambda|)^2 - \lambda^2 - (\hbar v_F k_x)^2}\,, \tag{73}$$

$\mu \in \{1, 2\}$.

The wave function of the transmitted electron is also decomposed by the two eigenfunctions $|\chi_{\mu,+}\rangle$,

$$\widetilde{\psi}_{E,k_x}(x, y) = \mathrm{e}^{\mathrm{i}k_x x}\Big[T_1\mathrm{e}^{\mathrm{i}k_y^1 y}|\chi_{1,+}(k_x, k_y^1)\rangle + T_2\mathrm{e}^{\mathrm{i}k_y^2 y}|\chi_{2,+}(k_x, k_y^2)\rangle\Big]\,, \tag{74}$$

with

$$\hbar v_F k_y^\mu = \sqrt{(\sqrt{E^2 - M^2v^4} + (-1)^\mu|\lambda|)^2 - \lambda^2 - (\hbar v_F k_x)^2}\,. \tag{75}$$

In the limit $M \to \infty$, the transmitted plane wave simplifies as

$$\widetilde{\psi}_{E,k_x}(x, 0) = \mathrm{e}^{\mathrm{i}k_x x}\widetilde{T}_1\begin{pmatrix}1\\ -s_\lambda\\ 1\\ -s_\lambda\end{pmatrix} + \mathrm{e}^{\mathrm{i}k_x x}\widetilde{T}_2\begin{pmatrix}1\\ s_\lambda\\ 1\\ s_\lambda\end{pmatrix} \tag{76}$$

and

$$\widetilde{\psi}_{E,k_x}(x, W) = \mathrm{e}^{\mathrm{i}k_x x}\widetilde{T}_1\begin{pmatrix}1\\ -s_\lambda\\ -1\\ s_\lambda\end{pmatrix} + \mathrm{e}^{\mathrm{i}k_x x}\widetilde{T}_2\begin{pmatrix}1\\ s_\lambda\\ -1\\ -s_\lambda\end{pmatrix}, \tag{77}$$

with $s_\lambda = \lambda/|\lambda|$. The different expressions at $y = 0$ and W originate from the different sign of $\hbar v_F k_y \to \pm\mathrm{i}Mv^2$ that has to be chosen to yield an exponential decay in the infinite mass region. It therefore only depends on whether one deals with the upper or lower boundary.

At the boundaries $y = 0$ and W, the four components have to be continuous to guarantee a continuous current, which leads to the following two sets of equations:

$$\psi_{E,k_x}(x, 0) = \widetilde{\psi}_{E,k_x}(x, 0), \quad \psi_{E,k_x}(x, W) = \widetilde{\psi}_{E,k_x}(x, W). \tag{78}$$

With $\psi_{E,k_x} = (\psi_1, \psi_2, \psi_3, \psi_4)^{\mathrm{T}}$, this translates to the familiar boundary condition from [27] for the two spin channels, respectively:

$$\left.\frac{\psi_1}{\psi_3}\right|_{y=0} = \left.\frac{\psi_2}{\psi_4}\right|_{y=0} = 1, \quad \left.\frac{\psi_1}{\psi_3}\right|_{y=W} = \left.\frac{\psi_2}{\psi_4}\right|_{y=W} = -1. \tag{79}$$

References

[1] Novoselov K S, Geim A K, Morozov S V, Jiang D, Zhang Y, Dubonos S V, Grigorieva I V and Firsov A A 2004 *Science* **306** 666
[2] Geim A K and Novoselov K S 2007 *Nat. Mat.* **6** 183
[3] Castro Neto A H, Guinea F, Peres N M R, Novoselov K S and Geim A K 2009 *Rev. Mod. Phys.* **81** 109
[4] Kane C L and Mele E J 2005 *Phys. Rev. Lett.* **96** 226801
[5] Min H, Hill J E, Sinitsyn N A, Sahu B R, Kleinman L and MacDonald A H 2006 *Phys. Rev.* B **74** 165310
[6] Huertas-Hernando D, Guinea F and Brataas A 2006 *Phys. Rev.* B **74** 155246
[7] Yao Y, Ye F, Qi X L, Zhang S-C and Fang Z 2007 *Phys. Rev.* B **75** 041401
[8] Boettger J C and Trickey S B 2007 *Phys. Rev.* B **75** 121402
[9] Gmitra M, Konschuh S, Ertler C, Ambrosch-Draxl C and Fabian J 2009 arXiv:0904.3315
[10] Hill E W, Geim A K, Novoselov K, Schedin F and Blake P 2006 *IEEE Trans. Magn.* **42** 2694
[11] Tombros N, Josza C, Popinciuc M, Jonkman H T and van Wees B J 2007 *Nature* **448** 571
[12] Nishioka M and Goldman A M 2007 *Appl. Phys. Lett.* **90** 252505
[13] Cho S, Chen Y-F and Fuhrer M S 2007 *Appl. Phys. Lett.* **91** 123105
[14] Ohishi M, Shiraishi M, Nouchi R, Nozaki T, Shinjo T and Suzuki Y 2007 *Jpn. J. Appl. Phys.* **46** L605
[15] Josza C, Popinciuc M, Tombros N, Jonkman H T and van Wees B J 2008 *Phys. Rev. Lett.* **100** 236603
[16] Wang W H, Pi K, Li Y, Chiang Y F, Wei P, Shi J and Kawakami R K 2008 *Phys. Rev.* B **77** 020402
[17] Goto H, Kanda A, Sato T, Tanaka S, Ootuka Y, Odaka S, Miyazaki H, Tsukagoshi K and Aoyagi Y 2008 *Appl. Phys. Lett.* **92** 212110
[18] Han W, Wang W H, Pi K, Li Y, McCreary K M, Bao W, Li Y, Lau C N and Kawakami R K 2009 *Phys. Rev. Lett.* **102** 137205
[19] Trauzettel B, Bulaev D V, Loss D and Burkard G 2007 *Nat. Phys.* **3** 192
[20] Ezawa M 2009 *Eur. Phys. J.* B **67** 543
[21] Brey L and Fertig H A 2007 *Phys. Rev.* B **76** 205435
[22] Ding K-H, Zhou G, Zhu Z-G and Berakdar J 2008 *J. Phys.: Condens. Matter* **20** 345228
[23] Onari S, Ishikawa Y, Kontani H and Inoue J-I 2008 *Phys. Rev.* B **78** 121403
[24] Rashba E I 2009 *Phys. Rev.* B **79** 161409
[25] Varykhalov A, Sánchez-Barriga J, Shikin A M, Biswas C, Vescovo E, Rybkin A, Marchenko D and Rader O 2008 *Phys. Rev. Lett.* **101** 157601
[26] Castro Neto A H and Guinea F 2009 *Phys. Rev. Lett.* **103** 026804
[27] Berry M V and Mondragon R J 1987 *Proc. R. Soc. Lond.* A **412** 53
[28] Huertas-Hernando D, Guinea F and Brataas A 2008 arXiv:0812.1921
[29] Peres N M R, Rodrigues J N B, Stauber T and Lopes dos Santos J M B 2009 *J. Phys.: Condens. Matter* **21** 344202
[30] Zarea M and Sandler N 2009 *Phys. Rev.* B **79** 165442